Proceedings of the 8th International Conference on Computing and Data Science
DOI: 10.54254/2755-2721/2026.37866

Adaptive Energy-Threshold DFT-LS Channel Estimation for Sparse MIMO-OFDM Systems

Jingrun Pei

School of Electronic Information and Communications, Huazhong University of Science and Technology, Wuhan, China
3631570964@qq.com

Abstract. Reliable channel state information supports coherent multiple-input multiple-output orthogonal frequency-division multiplexing (MIMO-OFDM) receivers. Least-squares channel estimation is simple but retains pilot noise, whereas fixed-window discrete Fourier transform least-squares (DFT-LS) denoising depends on a prescribed delay window. This paper proposes an adaptive energy-threshold DFT-LS refinement for sparse MIMO-OFDM channels. Cumulative delay-domain energy estimates a median-based tail noise floor, while amplitude thresholding selects taps over the full search interval. This separation prevents delayed weak taps from removal when an early strong tap satisfies the cumulative-energy condition. In sparse block-fading simulations with orthogonal pilots and uncoded quadrature phase-shift keying (QPSK), the proposed method reduces normalized mean-square error (NMSE) by approximately 42.3%–59.7% relative to fixed-window DFT-LS over 0–30 dB and reduces bit-error rate by 21.1% at 20 dB and 18.6% at 30 dB. The estimator remains non-iterative and requires less prior information than known-sparsity orthogonal matching pursuit (OMP-K) and oracle linear minimum mean-square error (Oracle-LMMSE) references.

Keywords: MIMO-OFDM, channel estimation, DFT-LS, sparse channel, adaptive thresholding

1. Introduction

Pilot-aided least-squares (LS) channel estimation requires little prior information but retains pilot noise. Discrete Fourier transform least-squares (DFT-LS) refinement suppresses delay-domain samples outside a prescribed window [1], and recent variants continue to improve DFT-domain accuracy and efficiency [2]. Its central tradeoff remains: a short window can remove delayed paths, whereas a conservative window retains unnecessary noise.

Delay-domain thresholding is established. Threshold pruning, two-stage noise-coefficient estimation, and adaptive MIMO-OFDM thresholds were studied in [3], [4, 5]; recent rules optimize bit-error rate (BER), use residual stopping, or exploit temporal support [6-8]. Thus, the distinction examined here is not thresholding itself, but using cumulative energy only for tail noise-floor estimation while selecting support over the full search interval.

© 2026 The Authors. This is an open access article distributed under the terms of the Creative Commons Attribution License 4.0 (https://creativecommons.org/licenses/by/4.0/).

DOI: 10.54254/2755-2721/2026.37866

Recent work also considers semi-blind estimation and pilot allocation [9, 10]. Fractional-delay leakage exposes the limits of DFT-bin support selection [11] and motivates gridless estimators [12]; these broader models are cited as context rather than like-for-like baselines for the present grid-aligned experiment.

The main contributions are: 1) an adaptive energy-threshold DFT-LS (AET-DFT-LS) estimator is formulated for sparse MIMO-OFDM channels; 2) the cumulative-energy index is used only to form a median-based tail noise-floor estimate, while the final sparse support is selected over the whole search interval; and 3) simulations compare the proposed estimator with LS, fixed-window DFT-LS, known-sparsity orthogonal matching pursuit (OMP-K), oracle linear minimum mean-square error (Oracle-LMMSE), and perfect channel state information (CSI) detection references.

2. System model and baselines

Consider an N_t -transmit and N_r -receive multiple-input multiple-output orthogonal frequency-division multiplexing (MIMO-OFDM) system with$N$ subcarriers and cyclic prefix (CP) length N_{cp} . The delay-domain channel between transmit antenna t and receive antenna r is denoted by $h_{r,t}[\ell]$, with $h_{r,t}[\ell] = 0$ for $\ell \geq L_{\max}$ and $N_{\mathrm{cp}} \geq L_{\max} - 1$. With j = $\sqrt{-1}$ denoting the imaginary unit, the corresponding subcarrier-domain channel is given by (1):

$$H_{r,t}[k] = \sum_{\ell=0}^{N-1} h_{r,t}[\ell] e^{-j2\pi k\ell/N} \tag{1}$$

Let $\mathbf{H}\left[k\right] \in \mathbb{C}^{N_r \times N_t}$ collect all transmit-receive links. For data symbol m, (2) gives the received signal:

$$y^{(m)}[k] = H[k]x^{(m)}[k] + w^{(m)}[k] \tag{2}$$

where $\mathbf{x}^{(m)}\left[k\right]$ is the transmitted quadrature phase-shift keying (QPSK) vector and $\mathbf{w}^{(m)}\left[k\right]$ is complex Gaussian noise.

The channel is block fading within one simulated frame. The receiver first estimates $\mathbf{H}[k]$ from the pilot blocks and then uses the resulting estimate for per-subcarrier linear minimum mean-square error (MMSE) detection of the following data symbols. This separates the channel-estimation problem from synchronization or coding effects and makes the BER metric reflect the quality of the estimated channel matrix used by the detector.

Orthogonal block pilots are used. During the pilot block of transmit antenna t , the remaining antennas are silent and a known pilot $p[k]$ is transmitted. The received pilot vector is given by (3):

$$y_{p,t}[k] = p[k]h_t[k] + w_{p,t}[k] \tag{3}$$

where $\mathbf{h}_t[k]$ is the t th column of $\mathbf{H}[k]$. The LS estimate is given by (4):

$$\widehat{h}_{t,LS}[k] = y_{p,t}[k]/p[k] \tag{4}$$

For a receive-transmit link, fixed-window DFT-LS first obtains $\widehat{h}_{r,t,\mathrm{LS}}\left[\ell\right]$ by an inverse DFT of $\widehat{H}_{r,t,\mathrm{LS}}\left[k\right]$, then keeps the first L_w taps, as defined in (5):

DOI: 10.54254/2755-2721/2026.37866

$$\widehat{h}_{r,t,DFT}[\ell] = \begin{cases} \widehat{h}_{r,t,LS}[\ell], & 0 \le \ell < L_w \\ 0, & L_w \le \ell < N \end{cases} \tag{5}$$

The limitation is that L_w is fixed before observing the sparse tap distribution.

3. Proposed AET-DFT-LS estimator

The proposed estimator operates independently on each antenna link. Let L_s be the delay-domain search length. It is a design parameter, not exact knowledge of the true channel length. Define the tap energy inside the search interval by (6):

$$e[\ell] = |\widehat{h}_{r,t,LS}[\ell]|^2, \quad 0 \le \ell < L_s \tag{6}$$

With ε > 0 used for numerical stabilization, the cumulative-energy ratio is given by (7):

$$C(q) = \frac{\sum_{\ell=0}^{q-1} e[\ell]}{\sum_{\ell=0}^{L_s-1} e[\ell] + \epsilon}, \quad q = 1, \ldots, L_s \tag{7}$$

and the cumulative-energy index is defined in (8):

$$\widehat{L} = \min\{q : C(q) \ge \rho\} \tag{8}$$

If the set is empty, $\widehat{L} = L_s$ is used.

Unlike strict cumulative-energy truncation, $\widehat{L}$ is not used as the final support boundary. It only selects the tail-energy set in (9) for noise-floor estimation:

$$\mathscr{E}_{tail} = \begin{cases} \{e[\ell] : \widehat{L} \le \ell < L_s\}, & \widehat{L} < L_s \\ \{|\widehat{h}_{r,t,LS}[\ell]|^2 : L_s \le \ell < N\}, & \widehat{L} = L_s, L_s < N \\ \{e[\ell] : 0 \le \ell < L_s\}, & otherwise \end{cases} \tag{9}$$

For complex Gaussian noise taps, the squared magnitude is exponentially distributed and its median equals the mean multiplied by log2. Hence the tap-noise power is estimated by (10):

$$\widehat{\sigma}_{tap}^2 = max\{median(\mathscr{E}_{tail})/log2, \epsilon\} \tag{10}$$

The amplitude threshold is $\eta = \alpha\sqrt{\widehat{\sigma}_{\text{tap}}^2}$, and the retained support is defined in (11):

$$\widehat{S} = \{\ell : 0 \le \ell < L_s,\ |\widehat{h}_{r,t,LS}[\ell]| > \eta\} \tag{11}$$

If $\widehat{\mathscr{S}}$ is empty, the largest tap in the search interval is retained. The retained delay taps are transformed back by an N -point DFT.

The per-link processing steps are summarized in Algorithm 1.

Algorithm 1: AET-DFT-LS estimator for one antenna link

Input: $\hat{H}_{\text{LS}}[k]$, L_s, ρ, α, ε

Output: $\hat{H}_{\text{AET}}[k]$

DOI: 10.54254/2755-2721/2026.37866

1. Obtain $\hat{h}_{LS}[\ell]$ by inverse DFT.
2. Compute $e[\ell]$ and $C(q)$ over $0 \le \ell < L_s$.
3. Find $\hat{L}$ from the cumulative-energy rule.
4. Form E_{tail} and estimate $\hat{\sigma}_{tap}^2$.
5. Select $\hat{S}$ by amplitude thresholding over $0 \le \ell < L_s$.
6. Keep taps in $\hat{S}$ and transform back to the frequency domain.

This design separates tail-noise estimation from support selection. A strong early path can make the cumulative-energy criterion hold before later weak paths appear. Testing all candidates inside L_s reduces this truncation risk while keeping the fast Fourier transform (FFT)-based structure of DFT-LS.

The separation also clarifies the role of the two design parameters. The parameter ρ affects where the tail samples are taken from and therefore influences the noise-floor estimate. The parameter α controls how aggressively the estimated noise floor is converted into an amplitude threshold. A larger α removes more delay-domain samples, but it may also discard weak channel taps if the threshold becomes too high. The fallback rule that keeps the largest tap when the support is empty prevents a degenerate all-zero estimate in very low-SNR or nearly empty observations.

4. Complexity and simulation results

LS has order $\mathcal{O}(NN_tN_r)$. DFT-LS and AET-DFT-LS both require one inverse DFT and one DFT per antenna link, giving the dominant order $\mathcal{O}(NN_tN_r\log N)$. AET-DFT-LS adds cumulative summation, a median-based tail estimate, and threshold scanning over L_s, which scales as $\mathcal{O}(L_sN_tN_r)$. OMP-K is implemented as a prior-assisted sparse reference using known sparsity K, while Oracle-LMMSE uses known maximum delay spread, power-delay profile (PDP), and noise variance.

The comparison therefore includes both computational and prior-information aspects. Fixed-window DFT-LS is fastest among the DFT-based refinements but depends on a window that should cover the true support. OMP-K can be highly accurate in sparse channels, but its use of known K is a favorable prior. Oracle-LMMSE is a statistical reference because it uses the PDP and noise variance. AET-DFT-LS is designed for the intermediate case where a search interval is available but the exact support or sparsity level is not. Table 1 summarizes these comparisons.

Table 1. Prior information and measured estimator-only runtime at 20 dB

Estimator	Main prior information	Runtime (μ s)
LS	Pilot only	6.20
DFT-LS	Window L_w	20.49
AET-DFT-LS	L_s, ρ, α	56.78
OMP-K	Known K	36.56
Oracle-LMMSE	PDP, L_{max} , noise variance	15.90

The simulation uses the frequency-domain equivalent MIMO-OFDM model under ideal synchronization and sufficient cyclic prefix length. A separate inverse FFT/cyclic-prefix (IFFT/CP) smoke comparison verified agreement with the complete ideal OFDM input-output relation, with relative error below 10^{-10}. The default setup, including the signal-to-noise ratio (SNR) range, is

DOI: 10.54254/2755-2721/2026.37866

summarized in Table 2. The AET parameters are selected from a preliminary grid as $\rho = 0.95$ and $\alpha = 1.6$.

For estimator a, the channel-estimation error is measured by (12):

$$NMSE_a = \frac{1}{F} \sum_{f=1}^{F} \frac{\sum_{k=0}^{N-1} \|\hat{H}_a^{(f)}[k] - H^{(f)}[k]\|_F^2}{\sum_{k=0}^{N-1} \|H^{(f)}[k]\|_F^2} \tag{12}$$

where F is the number of Monte Carlo frames, and ‖·‖_F denotes the Frobenius norm. The BER is computed after per-subcarrier MMSE detection by (13):

$$BER_a = N_{err,a} / N_{bit} \tag{13}$$

where $N_{\mathrm{err},a}$ is the number of QPSK bit errors, and N_bit is the total number of detected bits. Perfect CSI is excluded from the NMSE comparison because it is not an estimator; it is used only as a detection reference in the BER curve.

Table 2. Default simulation configuration

Parameter	Value
FFT size and CP length	N=64 , N_{cp}=16
MIMO size	N_t=N_r=2
Maximum delay and active paths	L_{max}=12, K=4
PDP parameter	τ=3
DFT and AET search lengths	L_w=L_s=16
AET parameters	ρ=0.95 , α=1.6
SNR range and frames	0:5:30 dB, 1000 frames

Figure 1(a) shows that AET-DFT-LS achieves lower simulated normalized mean-square error (NMSE) than LS and fixed-window DFT-LS over the tested SNR range. Relative to fixed-window DFT-LS, the AET-to-DFT NMSE ratio decreases from 0.577 at 0 dB to 0.403 at 30 dB, corresponding to an NMSE reduction of about 42.3%–59.7%. The improvement is larger at moderate and high SNR because the delay-domain noise floor is easier to separate from sparse channel taps. OMP-K gives lower high-SNR NMSE because it uses known sparsity K, and Oracle-LMMSE is interpreted as a statistical reference.

Figure 1(b) reports the corresponding BER. AET-DFT-LS reduces BER relative to fixed-window DFT-LS by about 21.1% at 20 dB and 18.6% at 30 dB. The perfect-CSI curve is included only as a detection reference. Table 1 shows that the adaptive thresholding step increases runtime relative to DFT-LS, but the estimator remains non-iterative and avoids the known-sparsity prior required by OMP-K.

DOI: 10.54254/2755-2721/2026.37866

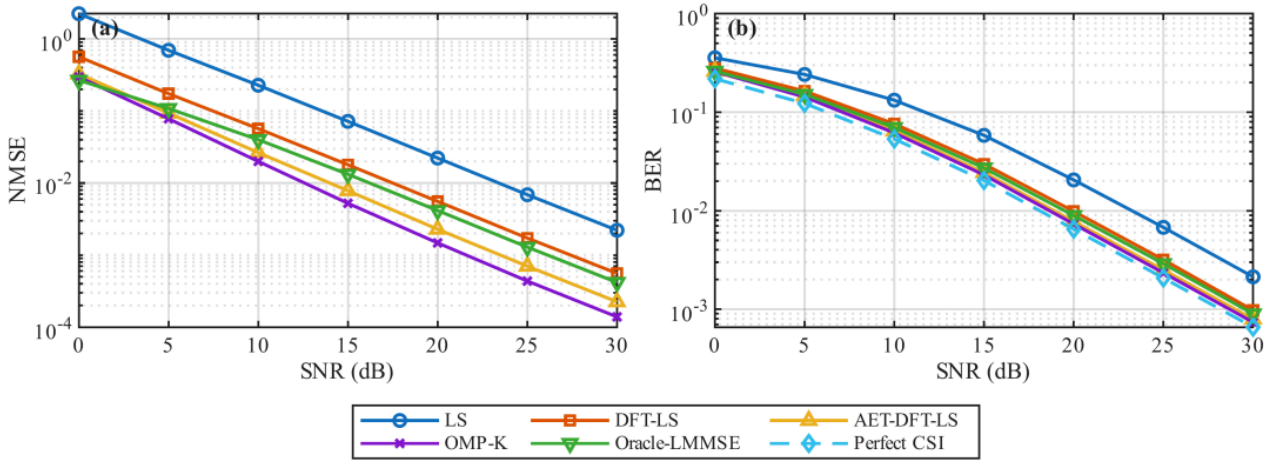


Figure 1. NMSE and BER comparison under sparse block-fading MIMO-OFDM settings

The BER gap between AET-DFT-LS and OMP-K is smaller than the corresponding NMSE gap, especially at moderate SNR. This is because detection errors depend on both channel-estimation error and residual receive noise. Once the channel estimate is accurate enough for the linear detector to suppress most inter-stream interference, additional NMSE reduction does not translate linearly into BER reduction. The main practical observation is therefore that AET-DFT-LS improves the fixed-window DFT-LS detector input without requiring the exact sparse support size.

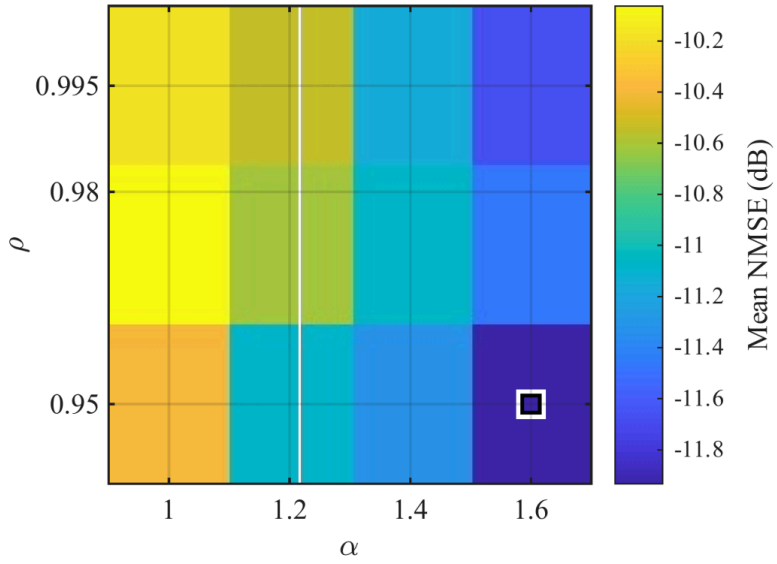


Figure 2. AET parameter sensitivity in terms of mean NMSE

Figure 2 shows the grid search used to select the AET parameters. The pair $\rho = 0.95$ and $\alpha = 1.6$ gives the lowest average NMSE in the tested grid, with mean NMSE 0.0641, high-SNR NMSE 0.00112, and 4.73 retained taps on average. Since the nominal number of active paths is $K = 4$, the retained-tap count indicates that the threshold is not simply preserving most of the search interval. Additional short sensitivity checks at 20 dB show that the AET-to-DFT NMSE reduction decreases

DOI: 10.54254/2755-2721/2026.37866

as the channel becomes less sparse or as $L_{\max}$ approaches L_s, which is consistent with the role of tail samples in the noise-floor estimate.

The additional sensitivity checks are used only to identify the operating boundary of the proposed rule. When the number of active paths is increased from $K = 2$ to $K = 8$, the NMSE reduction of AET-DFT-LS relative to fixed-window DFT-LS decreases from about 65.5% to 37.5%. This trend is expected because a denser channel contains fewer pure-noise taps inside the search window, leaving less room for adaptive tap removal. A similar effect appears when the maximum delay length is increased. For $L_{\max} = 8, 12$, and 16, the corresponding NMSE reductions are about 57.9%, 58.0%, and 27.8%, respectively. The smaller gain at $L_{\max} = 16$ occurs because the search interval is almost fully occupied by possible channel taps, so the tail set becomes less noise dominated.

The antenna-scale check also supports the per-link interpretation of the estimator. In both 2×2 and 4×4 settings, the AET-to-DFT NMSE ratio at 20 and 30 dB remains in the range of about 0.41–0.43. This indicates that increasing the number of antenna pairs mainly increases the number of independently processed links, rather than changing the delay-domain denoising mechanism. These results do not prove robustness for all channels, but they show that the main gain is consistent with the intended sparse-tap selection behavior in the tested settings.

5. Discussion

The proposed estimator is most useful when the receiver can define a conservative delay search interval but cannot specify the exact sparse support. In this case, fixed-window DFT-LS must either keep the whole interval and preserve noise or shorten the window and risk deleting delayed paths. AET-DFT-LS keeps the same search interval but makes a tap-wise decision relative to an estimated tail noise floor. This is why the method improves over fixed-window DFT-LS in the sparse block-fading experiments while still remaining much simpler than iterative sparse Bayesian estimators.

The method also has clear limitations. If the channel becomes dense inside the search interval, many delay samples contain valid channel energy and the number of removable noise-only taps decreases. If the true delay spread approaches L_s, the samples used for tail-noise estimation may include weak valid paths, reducing threshold selectivity. Thus, the method should be interpreted as an adaptive DFT-LS refinement for sparse channels, not as a universal replacement for statistical or sparse-recovery estimators.

From an implementation viewpoint, the estimator can be inserted after any pilot-aided LS channel estimate that provides a uniformly sampled frequency response. It does not change the pilot structure, data detector, or OFDM modulation. The additional operations are performed per transmit-receive link in the delay domain: cumulative summation, median calculation over the tail set, and threshold comparison over L_s. These operations are easy to vectorize and require only the three scalar design parameters L_s, ρ, and α. This makes the method suitable for receiver designs where a small increase in post-processing cost is acceptable but exact channel statistics are not available.

6. Conclusion

This paper proposed AET-DFT-LS channel estimation for sparse MIMO-OFDM systems. The method uses cumulative tap energy to estimate a tail noise floor, but selects the final support by thresholding over the full search interval. This separates noise-floor estimation from the final sparse-tap decision and avoids using the cumulative-energy index as a hard truncation boundary.

Simulations show lower NMSE and BER than LS and fixed-window DFT-LS in the considered sparse block-fading settings, with less prior information than OMP-K and Oracle-LMMSE. The

DOI: 10.54254/2755-2721/2026.37866

present study assumes ideal synchronization, sufficient cyclic prefix length, orthogonal pilots, and uncoded QPSK. Future work will test the method under time-varying channels, standardized channel models, synchronization errors, and coded transmission.

References

[1] Edfors, O., Sandell, M., van de Beek, J.-J., Wilson, S. K., & Börjesson, P. O. (2000). Analysis of DFT-based channel estimators for OFDM. *Wireless Personal Communications, 12*(1), 55–70. https://doi.org/10.1023/A:1008864109605

[2] Dziwoki, G., Izydorczyk, J., & Kucharczyk, M. (2025). Enhanced OFDM channel estimation via DFT-based precomputed matrices. *Electronics, 14*(17), 3378. https://doi.org/10.3390/electronics14173378

[3] Oliver, J., Aravind, R., & Prabhu, K. M. M. (2008). Sparse channel estimation in OFDM systems by threshold-based pruning. *Electronics Letters, 44*(13), 830–832. https://doi.org/10.1049/el:20081089

[4] Xie, H., Andrieux, G., Wang, Y., Diouris, J.-F., & Feng, S. (2014). Efficient time domain threshold for sparse channel estimation in OFDM system. *AEU–International Journal of Electronics and Communications, 68*(4), 277–281. https://doi.org/10.1016/j.aeue.2013.09.005

[5] Zhang, M., Zhou, X., & Wang, C. (2020). Time-varying sparse channel estimation based on adaptive average and MSE optimal threshold in STBC MIMO-OFDM systems. *IEEE Access, 8*, 177874–177895. https://doi.org/10.1109/ACCESS.2020.3026210

[6] Yang, X., Zhou, Y., Tong, F., & Zheng, H. (2024). Minimum-BER sparsity exploitation estimation of time-varying underwater acoustic OFDM communication channel. *IEEE Internet of Things Journal, 11*(17), 29089–29101. https://doi.org/10.1109/JIOT.2024.3406370

[7] Chové, T., Bouvet, P.-J., Laot, C., & Le Josse, N. (2025). A new adaptive stopping criterion for sparse channel estimation in MIMO-OFDM underwater acoustic communications. In *Proc. OCEANS 2025 Brest* (pp. 1–7). doi: 10.1109/OCEANS58557.2025.11104647.

[8] Xie, H., Wang, Y., Andrieux, G., & Men, S. (2026). Efficient high-resolution sparse channel estimation based on temporal correlation in MIMO-OFDM systems. *Sensors, 26*(10), 3136. doi: 10.3390/s26103136.

[9] Mehrabani, M. R., Abolhassani, B., & Haddadi, F. (2024). Semi-blind channel estimation and pilot allocation for doubly-selective massive MIMO-OFDM systems. *IEEE Access, 12*, 111565–111578. doi: 10.1109/ACCESS.2024.3441375.

[10] Zhou, Y., Gu, Z., Wang, S., Yang, Y., & Fan, P. (2025). Non-uniform pilot pattern design for sparse channel estimation in MIMO-OFDM systems. *IEEE Trans. Veh. Technol., 74*(2), 3039–3051. doi: 10.1109/TVT.2024.3481014.

[11] Qiao, G., Qiang, X., Wan, L., & Jia, H. (2024). Energy leakage in OFDM sparse channel estimation: The drawback of OMP and the application of image deblurring. *Digit. Commun. Netw., 10*(5), 1280–1288. doi: 10.1016/j.dcan.2023.08.003.

[12] Zhu, L., et al. (2025). A novel gridless uplink/downlink channel estimation method for millimeter wave MIMO-OFDM systems. *IEEE Trans. Wireless Commun., 24*(5), 3780–3793. doi: 10.1109/TWC.2025.3539001.